Determination of gas-temperature and velocity profiles in an argon thermal-plasma jet by laser-light scattering

S. C. Snyder, L. D. Reynolds, G. D. Lassahn, J. R. Fincke, and C. B. Shaw, Jr.
Idaho National Engineering Laboratory, EG&G Idaho, Inc., P.O. Box 1625, Idaho Falls, Idaho 83415

R. J. Kearney
Department of Physics, University of Idaho, Moscow, Idaho 83843
(Received 13 April 1992)

Gas-temperature and velocity profiles at the exit plane of a thermal argon plasma torch have been determined directly from a high-resolution Doppler-shifted line-shape analysis of laser light scattered by the plasma. Peak temperature and velocity values observed were 13 350 K±7% and 1100 $m s^{-1}$±3%. Velocities as low as 45 $m s^{-1}$±45% were measured in the fringe of the jet. An injection-seeded pulsed neodymium-doped yttrium aluminum garnet laser was used as the laser source and the scattered laser light was analyzed with a scanning tandem Fabry-Pérot interferometer. Temperature data obtained from laser scattering are compared with values obtained from emission spectroscopy and show a severe departure from local thermodynamic equilibrium (LTE) in the outer regions of the jet. Gas temperatures were observed to increase as the torch operating current increased from 300 to 500 A, but remained constant as the operating current increased to 900 A. However, electron temperatures and densities continued to increase with operating current. This suggests that increasing the electrical power drives the plasma away from LTE. Measured temperature and velocity profiles were found to be nearly parabolic.

PACS number(s): 52.70.Kz, 52.75.Hn, 52.25.Rv, 42.62.Fi

INTRODUCTION

The most important parameter describing an atmospheric pressure thermal plasma is the gas or kinetic temperature. The problem of determining the true gas temperature of a thermal plasma has occupied researchers for many years [1–3]. The traditional approach is to relate the measured intensity of emission lines to the gas or kinetic temperature of the atoms through the assumption of local thermodynamic equilibrium (LTE). If the assumption of LTE is valid, electrons and heavy particles have the same unique temperature, the population of excited states is described by Maxwell-Boltzmann statistics, and, except for radiative processes, the principle of detailed balance applies.

Since excitation processes in thermal plasmas are dominated by electron collisions, LTE does not occur unless there is a critical electron density. It is estimated that a critical electron density of 10^{23} m^{-3} is required for LTE to occur [4,5], although recent theoretical work [6] suggests this number is an order of magnitude low. Further departure from LTE has been shown to result from resonance radiation trapping [7,8], which produces excited-state populations greater than those predicted by LTE. In addition, electron diffusion resulting from large temperature gradients within the plasma can cause a departure from the LTE if the time for diffusion to occur over a path length is less than the time for equilibrium to be established [9].

A more realistic description of thermal plasmas is most likely given by the partial local thermodynamic-equilibrium (PLTE) model [9,10]. This model assumes that free electrons are in equilibrium with the populations of the upper atomic excited states, but not necessarily in equilibrium with the ground state. The details of this theory are dependent mainly on the strength of the electron-atom interactions and excited-state radiative decay rates. Emission spectroscopy may be useful for determining electron temperature if the plasma is in PLTE, but cannot determine gas temperatures because collisional and radiative processes have not been adequately quantified.

High-resolution line-shape analysis of laser light elastically scattered by the plasma allows direct and unintrusive measurement of the plasma gas temperature and velocity. Interpretation of line-shape data does not depend on LTE assumptions or reliance on non-LTE models. Also, a high degree of spatial resolution is possible and there is no need for Abel inversion of the data, as with emission spectroscopy. At atmospheric pressure for electron densities greater than 10^{22} m^{-3}, Thomson scattering dominates, while at lower electron densities, Rayleigh scattering dominates. If the difference between the scattered light wave vector and the incident laser wave vector has a component along the flow velocity, the line shape will be Doppler shifted relative to the incident laser frequency and the gas velocity can be readily determined.

Ion-component line shapes obtained by heterodyne detection of Thomson-scattered CO_2 laser light [11,12] have been successfully used to determine temperatures of low-pressure, high-current transferred arcs. Gas velocities have been determined from Doppler-shifted line-shape measurements made on a high-current, atmospher-

ic pressure transferred arc using a Q-switched ruby laser and scanning Fabry-Pérot interferometer (FPI) [13] and more recently on a plasma jet using a double pulsed dye laser and scanning FPI in conjunction with a monochromator [14]. Gas temperatures from some very high-quality line shapes made in a transferred arc have also been recently been reported using a tunable narrow bandwidth dye laser as the laser source and a monochromator for spectral analysis [15].

Radial temperature and gas-velocity profiles near the torch exit are of practical importance as boundary conditions for computational modeling of the momentum-energy balance and energy transport of the plasma flow downstream. Velocity profiles are usually calculated from spectroscopic temperature profiles using conservation of mass and thermal energy [16]. If the temperature profiles are not accurate, the velocity profiles will be unrealistic. Laser Doppler anemometry has been used to extrapolate gas velocity from the velocity of small particles injected into the plasma [17]. However, this approach is intrusive, small particles do not survive exposure to high-temperature plasma, and it is questionable whether the particle velocity accurately represents the gas velocity.

We report in this paper results of recent measurements of gas-temperature and gas-velocity profiles of an atmospheric pressure argon thermal plasma jet obtained from the line-shape analysis of scattered laser light. A frequency-doubled injection-seeded Nd:YAG laser (where YAG denotes yttrium aluminum garnet) was used as the source. The scattered light was spectrally analyzed using a scanning tandem Fabry-Pérot interferometer.

THEORY

It is well known that scattering of electromagnetic radiation by a medium is due to density fluctuations within the medium [18,19]. In the case of ionized gases, density fluctuations of the atoms and ions give rise to Rayleigh scattering, while density fluctuations of the free electrons give rise to Thomson scattering. Density fluctuations of the free electrons have two components, one resulting from the thermal motion of the electrons themselves, and the other due to electrostatic interactions with moving ions. The total scattered light signal from a thermal plasma is therefore a combination of Rayleigh scattering from atoms and ions, and Thomson scattering from free electrons. The spatial radiation pattern of both Rayleigh and Thomson scattered light is that of the oscillating electric dipole.

Thomson scattering is characterized by the parameter

$$\alpha=\frac{1}{k\lambda_D} , \tag{1}$$

where $\lambda_D=(\epsilon_0 k_B T_e/n_e e^2)^{1/2}$ is the Debye length in the plasma and k is the magnitude of the difference between the scattered wave vector and the incident wave vector ($\mathbf{k}=\mathbf{k}_s-\mathbf{k}_0$). In the above equation, ϵ_0 is the permittivity of free space, k_B Boltzmann's constant, T_e the electron temperature, n_e the electron density, and e the electron charge. Since Thomson scattering is elastic, $|\mathbf{k}_s|=|\mathbf{k}_0|$, and so

$$k=\frac{4\pi\sin\theta/2}{\lambda_0} , \tag{2}$$

where θ is the scattering angle and λ_0 the wavelength of the incident laser light.

Since electron density fluctuations have spatial and time dependence, they can be Fourier transformed to functions of $\mathbf{k}$ and ω, where ω is, in this case, the difference between the angular frequency of the scattered light and the angular frequency of the incident laser. Momentum is conserved during scattering, so only the specific component of the density fluctuation with a wave vector $\mathbf{k}$ participates. When the wavelength of the density fluctuation is much less than the Debye length, $\alpha\ll 1$ and the electron motion appears to be uncorrelated and is referred to as incoherent Thomson scattering. If the wavelength is longer than the Debye length, collective effects become important and influence the spectrum of scattered light. Scattering from correlated electrons is referred to as coherent Thomson scattering.

The total spectral distribution of Thomson scattered light, determined by the electron and ion components of the free-electron density fluctuations, is

$$S(\mathbf{k},\omega)d\omega=S_e(\mathbf{k},\omega)d\omega+S_i(\mathbf{k},\omega)d\omega . \tag{3}$$

Assuming the electrons and ions obey Maxwellian velocity distributions characterized by an electron temperature T_e and ion temperature T_i, and that $T_e/T_i\geq 1$, but not much greater, Salpeter [20–22] approximated the electron and ion components of the coherent Thomson scattering spectral distribution functions appearing in Eq. (3) to be

$$S_e(\mathbf{k},\omega)d\omega=\pi^{-1/2}\left|\frac{1}{1+\alpha^2 W(x_e)}\right|^2\exp(-x_e^2)dx_e \tag{4}$$

and

$$S_i(\mathbf{k},\omega)d\omega=Z\pi^{-1/2}\left[\frac{\alpha^2}{1+\alpha^2}\right]^2\left|\frac{1}{1+\beta^2 W(x_i)}\right|^2 \times\exp(-x_i^2)dx_i , \tag{5}$$

where

$$x_{e,i}=\omega/[k(2k_B T_{e,i}/m_{e,i})^{1/2}] ,$$

$$\beta^2=Z[\alpha^2/(1+\alpha^2)]T_e/T_i ,$$

$$W(x_{e,i})=1-2x_{e,i}\exp(-x_{e,i}^2)\int_0^{x_{e,i}}\exp p^2 dp -[i\pi^{1/2}x_{e,i}\exp(-x_{e,i}^2)] ,$$

Z is the degree of ionization, and $m_{e,i}$ the electron or ion mass, respectively. An example of a theoretical line shape of the ion feature of coherent Thomson scattering from a hypothetical plasma with $T_e=15\,000$ K, $T_i=13\,000$ K, $n_e=6.4\times10^{22}$ m^{-3}, 532.0-nm laser wavelength, and 80° scattering angle ($\alpha=2.0$) is presented in Fig. 1. The two humps in the line shape are due to scattering from ion acoustic waves in the plasma. As α decreases and collective effects become less important,

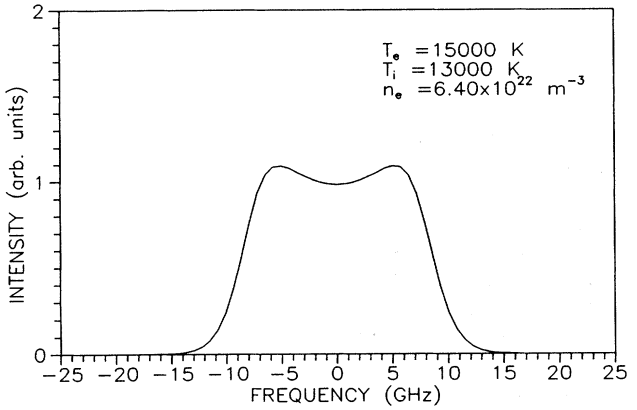

FIG. 1. Theoretical ion feature line shape for a hypothetical plasma with $T_e = 15\,000$ K, $T_i = 13\,000$ K, and $n_e = 6.4 \times 10^{22}$ m^{-3} ($\alpha = 2$).

this structure disappears.

The spectral distribution of Rayleigh scattered light from gases depends on a parameter y that is analogous with α and given by

$$y = \frac{1}{k\lambda_l} , \tag{6}$$

where λ_l is the collisional mean free path. If $y < 0.1$, the line shape of Rayleigh scattered light is described [23] by a simple Gaussian function with a full width at half maximum of

$$\Delta\omega = 4(2k_B T \ln 2/mc^2)^{1/2}\omega_0 \sin\theta/2 , \tag{7}$$

where ω_0 is the angular frequency of the incident laser light, m the mass of the scattering atom, c the speed of light, and T the gas temperature, assumed equal to T_i.

The frequency spread of the electron component of Thomson scattered light is 200–300 times greater than the frequency spread of the ion component. As a result, the electron component is ignored in this experiment, and we concentrate on measuring the superposition of the ion component with Rayleigh scattering from neutral and singly ionized argon.

It has been shown theoretically and experimentally [24–26] that ion-ion and ion-neutral collisions in the plasma can greatly effect the electron density fluctuations and accordingly influence the spectral distribution of coherent Thomson scattered light. The effect of collisions is characterized by a parameter also analogous to α, defined as

$$p = 1/k\lambda_{\mathrm{MFP}} , \tag{8}$$

where λ_{MFP} is the mean free path of ion-ion and ion-neutral collisions. If $p \geq 1$, collisional effects dominate the spectrum of scattered light. For our experimental conditions, $p \leq 0.1$ and we ignore any effects due to collisions.

Examining the total scattered light signal, integrated over all frequencies, gives insight into the relative contributions of the ion component of Thomson scattering and Rayleigh scattering to the total signal strength. Integrating Eq. (3) over all frequencies gives [20]

$$S_i(\mathbf{k}) = \frac{Z\alpha^4}{(1+\alpha^2)[1+\alpha^2+Z\alpha^2(T_e/T_i)]} . \tag{9}$$

The total integrated signal strength from an argon plasma, normalized to the Rayleigh signal strength from argon under ambient conditions, is then [27]

$$I_{\mathrm{tot}} = \frac{I_R^0}{n_a^0 \sigma_R}[n_a\sigma_R + n_+\sigma_+ + n_1\sigma_1 + n_e\sigma_t S_i(\mathbf{k})] , \tag{10}$$

where I_R^0 is the intensity of Rayleigh scattered light from ambient argon, n_a^0 the number density of argon atoms under ambient conditions, n_a the number density of ground-state neutral argon, n_+ the ion number density (we assume $n_+ = n_e$), n_1 the number density of the argon $4p'[3/2]$ excited state at 107 290 cm^{-1}, σ_R the Rayleigh scattering cross section for ground-state neutral argon ($\sigma_R = 5.24 \times 10^{-32}$ $m^2 sr^{-1}$ for $\lambda_0 = 532.0$ nm), σ_+ the Rayleigh scattering cross section for singly ionized argon ($\sigma_+ \approx 0.5\sigma_R$) [28], σ_1 the Rayleigh scattering cross section for the $4p'[3/2]$ excited state of neutral argon at 107 290 cm^{-1}, and σ_T the Thomson scattering cross section ($\sigma_T = 7.94 \times 10^{-30}$ $m^2 sr^{-1}$). The $4p'[3/2]$ excited state of argon is included because the wavelength of the laser used in this experiment is nearly resonant with the $4p'[3/2]$ to $7d'[5/2]^\circ$ transition at 531.8 nm. Near-resonant Rayleigh scattering cross sections can be several orders of magnitude larger than the nonresonant cross sections, and in this case, σ_1 has been estimated [29] to be about $840\sigma_R$. However, the number density of atoms in the $4p'[3/2]$ state in the temperature range of this experiment is so low that the contribution of near resonant Rayleigh scattering to the total signal is not important. A plot of the total integrated signal intensity versus temperature as calculated from Eq. (9) using the assumption of LTE is given in Fig. 2.

The plasma jet velocity $\mathbf{v}$ is determined directly from the Doppler shift of the scattered light by

$$\Delta\omega = \mathbf{k}\cdot\mathbf{v} . \tag{11}$$

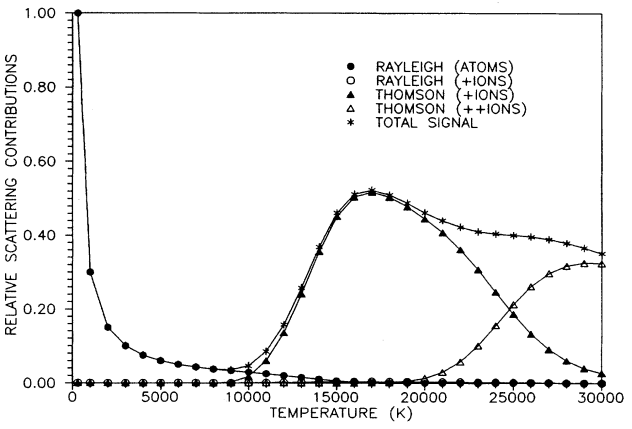

FIG. 2. Total integrated intensity of scattered light normalized to Rayleigh scattering from ambient argon.

EXPERIMENT

The plasma jet studied was generated in a commercial plasma torch operated with argon and discharged into ambient air. The torch schematic is depicted in Fig. 3. The background radiation from the resulting thermal plasma is very intense and the scattered light signal relatively weak. Consequently, high-resolution line-shape measurements with a good signal-to-noise ratio require the use of high peak power, narrow linewidth laser sources. In the work reported here a pulsed, injection-seeded Nd:YAG laser was used. The Nd:YAG laser generates 10-ns pulses that have nearly transformed limited bandwidths of approximately 100 MHz. The output was frequency doubled to a wavelength of 532.0 nm. A single-pass tandem FPI, supplied by Sandercock [30], was used for the high-resolution spectral analysis of the scattered light. The tandem FPI, comprised of two FPI's mounted in series on a deformable parallelogram stage, as shown in Fig. 4, is piezoelectrically scanned. Because of the layout geometry, the plate separation of the second cavity differs from that of the first cavity by a constant $\cos\theta_0$ factor. Hence only transmission orders of the first cavity that overlap with transmission orders of the second cavity pass through the instrument, and the effective free spectral range of the FPI is greatly expanded. More importantly, the resolving power R of the multiple cavity FPI increases according to [31]

$$R \propto (\mathcal{F}/2)^p , \tag{12}$$

where $\mathcal{F}$ is the finesse of a single cavity, and p the number of cavities in the series. Unfortunately, the laser wavelength was somewhat outside of the range of maximum reflectivity of the available FPI mirrors (93% from 480–520 nm). As a result, the total effective finesse of the instrument was only approximately 25.

The schematic of the experiment is depicted in Fig. 5. A small amount of laser light was split off of the main beam and focused into the FPI to act as a frequency reference from which Doppler shifts due to the gas velocity are measured. The output of the FPI was detected with a photomultiplier tube and boxcar averager synchronized to the firing of the laser. The single shot output of the boxcar was digitized by an analog-to-digital converter and stored on a computer. The FPI was scanned over a frequency interval of approximately 60 GHz centered about the laser frequency. A single scan, consisting of 90 laser shots was completed in approximately 5 s. Line shapes typically represents the average of 50 successive scans. The incident laser beam was focused in the plasma to a waist diameter of approximately 100 μm. The entrance aperature of the FPI was a 400-μm pinhole giving a spatial resolution of approximately 3×10^{-3} mm^3. The plasma jet was operated vertically with the scattered light collected at an angle of $10°\pm1°$ from the flow axis giving a scattering angle of $80°\pm1°$. A 0.3-nm bandwidth interference filter centered at 532.0 nm was used to reduce the plasma background. A half-wave plate was used to rotate the polarization of the laser beam to maximize the scattering signal and verifying that the dependence of the signal intensity on the polarization angle was characteristic of oscillating electric dipoles and not stray light. The laser pulse rate was 20 Hz with a pulse energy of 200 mJ. The resulting energy density was high, but did not influence the measured temperature values.

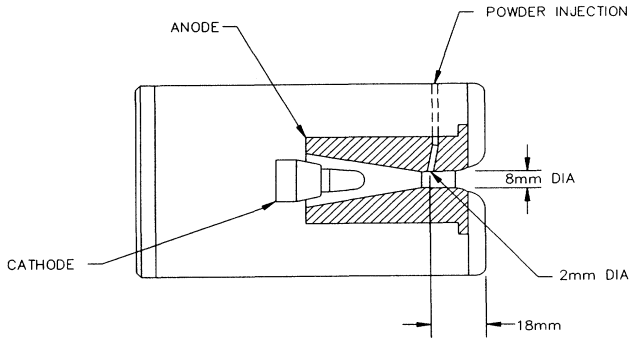

FIG. 3. Plasma-torch schematic.

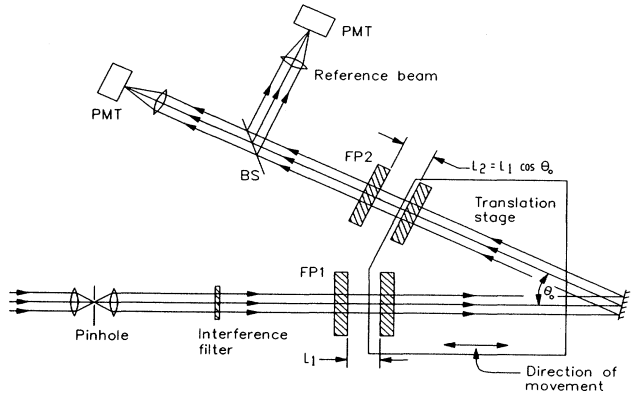

FIG. 4. Schematic of tandem Fabry-Pérot interferometer (Ref. [30]). PMT denotes a photomultiplier tube.

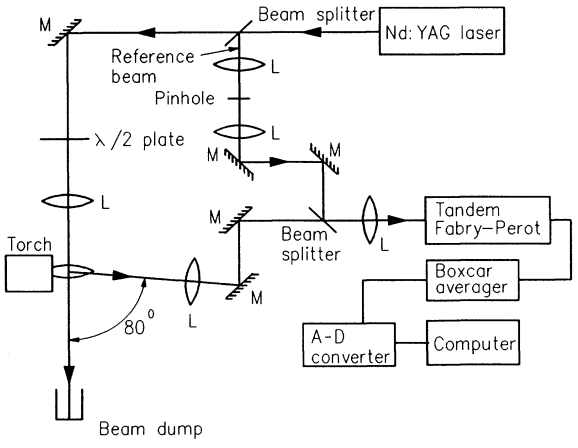

FIG. 5. Experimental setup. A-D converter denotes an analog-to-digital converter.

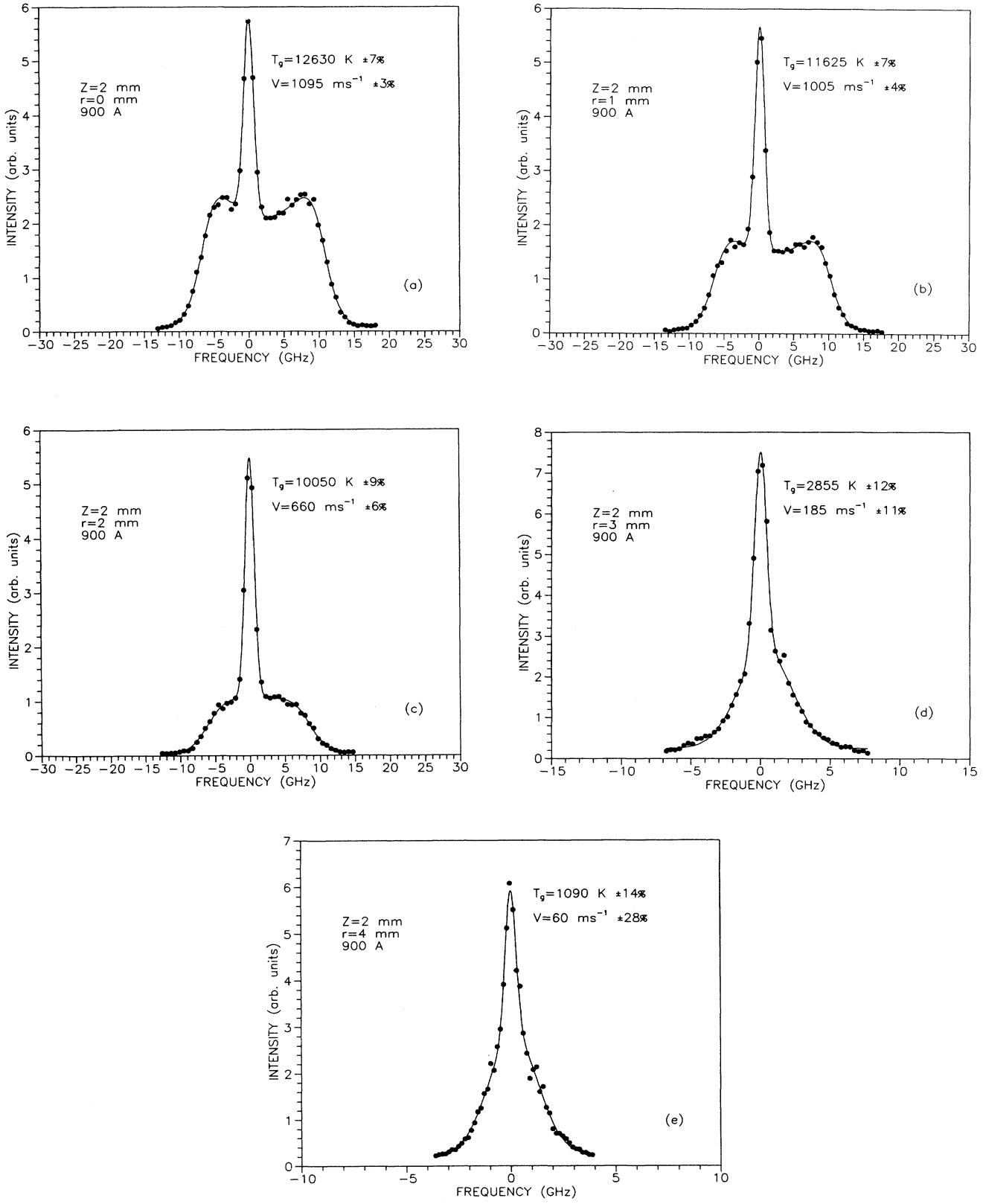

FIG. 6. (a)–(e) Line shape of scattered light as a function of radius for 900-A operating current. Data were taken at an axial position of 2 mm downstream from the torch face. The argon gas flow rate was 35.4 l min^{-1}. The solid curve represents the least-squares fit of the data to the theory.

RESULTS AND DISCUSSION

The plasma torch operating conditions were 35.4 $l\,min^{-1}$ argon-gas flow rate and currents ranging from 300 to 900 A. The electrical power dissipated in the torch increased linearly from 7.2 kW at 300 A to 22.9 kW at 900 A. Line-shape data were taken at an axial position of 2 mm downstream from the torch face. The resulting line shapes as a function of radius are presented in Figs. 6(a)–6(e) for the 900-A case. The central narrow peak in the line shapes is the FPI response to the reference laser beam. The curve represents the least-squares fit of the data to the theory, which is a superposition of the Thomson scattering and Rayleigh-scattering line shapes. The uncertainties of the temperature and velocity results in the center of the jet are approximately 5%, reflecting the high quality of the line-shape data. These uncertainties represent fitting errors, uncertainty of the scattering angle, and, in the case of the temperature values, uncertainty introduced in deconvoluting the instrument response function of the FPI from the line shapes [32].

Because of the dependence of the ion feature line shape on n_e, T_e, and T_i, these are the adjustable parameters for the curve fitting routine, along with the peak amplitude and center position of the line shape of the reference beam from which the flow velocity was determined. Since n_e and T_e are related by the ideal gas law, the partial pressure of the electron gas must be known if they are to be treated as independently adjustable parameters. This information was unknown and consequently it was necessary to fix the value of T_e at a reasonable value and then fit the ion component of the data while adjusting the values of n_e and T_i.

The value of the ion temperature resulting from the fit of the data to the theory is dependent on the fixed value of T_e, but this dependence is very weak. For example, a change of 4000 K in the fixed value of the electron temperature produced typically a change in the fitted value of T_i of approximately 30 K. If the value of the electron temperature was fixed at 20 000 K (T_e in thermal plasma jets is less than 15 000 K, so this upper bound is excessively high) the added uncertainty to the value of T_i was only approximately 0.2%. In practice, the value of T_e was set to 15 000 K for the analysis of all line shapes with a significant Thomson component [Figs. 6(a)–6(c)]. Because of its strong dependence on T_e, it is not possible to determine n_e accurately from ion feature line-shape data.

Temperature versus radius for the 300-, 500-, and 900-A data are shown in Figs. 7–9, respectively. There is experimental evidence [33] that plasma jets entrain cold gas from the surrounding atmosphere into the outer regions of the jet, where in the case of air, it can dissociate. This is particularly true at lower operating currents such as 300 A where the jet is more turbulent. As a result, the Rayleigh-scattering line shape is a superposition of Rayleigh scattering from argon and from atomic or molecular nitrogen, depending on the gas temperature. In principle, the amplitudes of these contributions could be treated as separate adjustable parameters so that knowledge of concentrations and scattering cross sections are not required. In practice, it was not possible to separate the effects of neutral argon and nitrogen, so the Rayleigh line shape for atomic nitrogen was not included explicitly. For the data in which atomic nitrogen is expected to contribute to the observed spectra, the significantly broader nitrogen contribution is unavoidably treated as an additional argon ion or atom contribution, resulting in artificially high temperatures. We believe this effect is evident in the 300-A data at the $r \geq 1$ mm radial positions. Entrained molecular species were seen to affect all data at the 4-mm radial location. Entrained air has no effect on the velocity data. Radial temperature

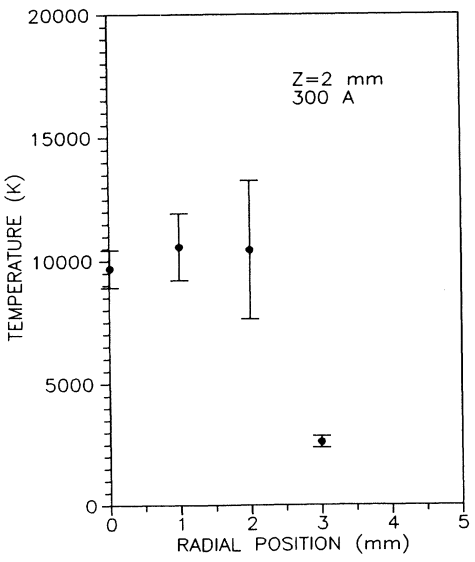

FIG. 7. Temperature distribution for 300-A operating current.

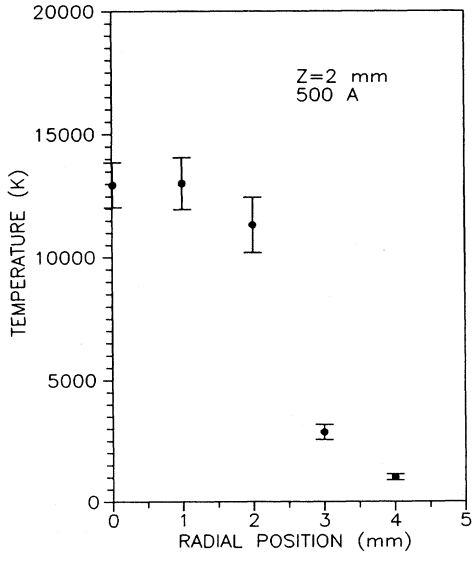

FIG. 8. Temperature distribution for 500-A operating current.

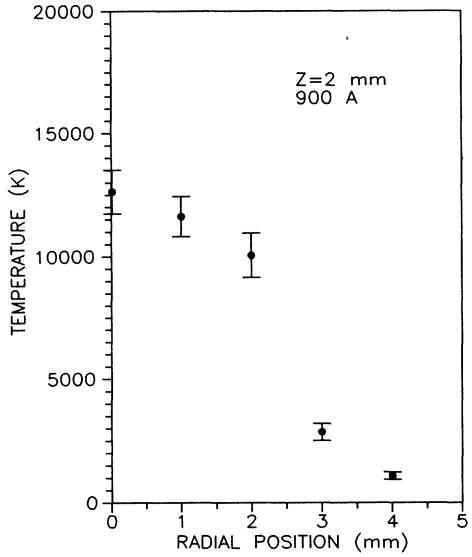

FIG. 9. Temperature distribution for 900-A operating current.

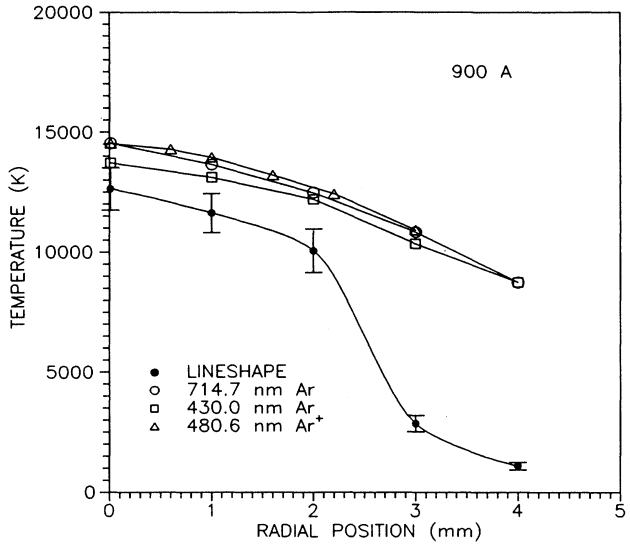

FIG. 11. Temperature distribution for 900-A operating current determined from LTE emission spectroscopy.

profiles determined assuming LTE from absolute emissivity measurements [34] of the neutral argon $5p[5/2]$ to $4s[3/2]^\circ$ and the $4p'[3/2]$ to $4s[3/2]^\circ$ transitions at 430.0 and 714.7 nm, respectively, and the singly ionized argon $4p\ ^4P^\circ$ to $4s\ ^4P$ transition at 480.6 nm for the 500- and 900-A operating currents are plotted in Figs. 10 and 11 with the results of the line-shape measurements. The uncertainties of the emission temperature measurements are estimated to be 5%. The details of these measurements are described elsewhere [16]. The temperatures determined by emission spectroscopy are assumed to be representative of electron temperatures since according to the PLTE theory the upper Ar levels are probably in equilibrium with T_e. The data show a significant departure from LTE in the outer regions of the jet. This is probably due to the effects of radiation trapping by ground-state argon atoms and electron diffusion.

A plot of the center-line ($r=0$ mm) gas temperature and velocity as a function of current is given in Fig. 12. It is interesting to note that both the temperature and velocity initially increase steadily with current, but then roll off and remain essentially constant above 600 A. As the current increases from 600 to 900 A, the electrical power dissipated in the torch increases approximately 60% without increasing the gas temperature or velocity. The torch efficiency as a function of current decreases somewhat at the higher currents, but this does not account for the saturation of the temperature and velocity. Some insight into this observation can be gained from the center-line spectroscopic values of T_e and n_e as a function of

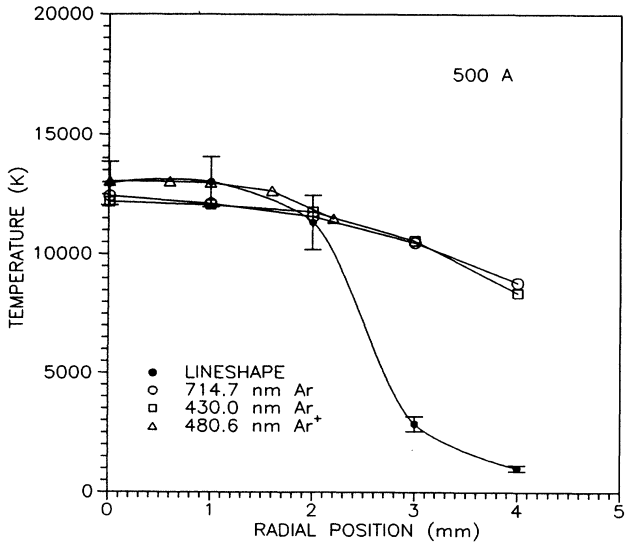

FIG. 10. Temperature distribution for 500-A operating current determined from LTE emission spectroscopy.

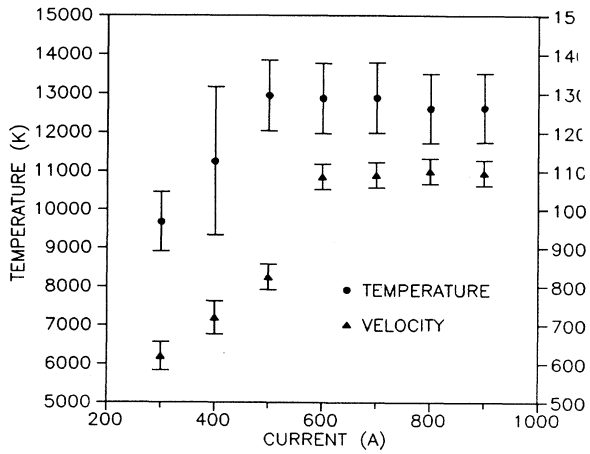

FIG. 12. Center-line ($r=0$ mm) temperature and velocity as a function of operating current at an axial location 2 mm downstream from the torch face.

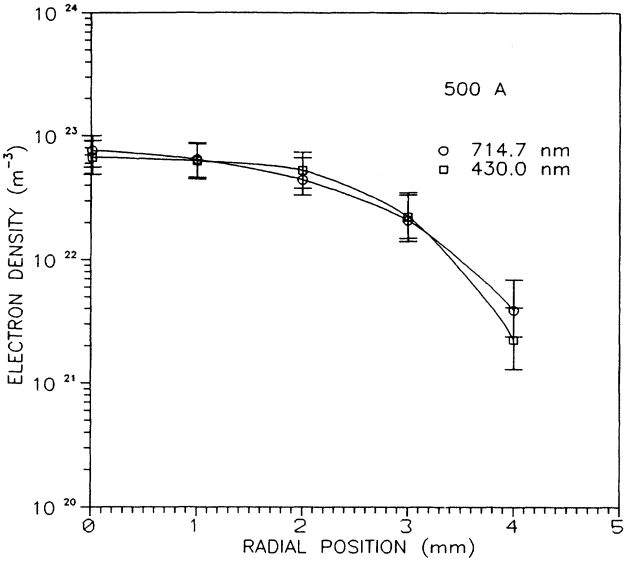

FIG. 13. Radial electron density profile for 500-A operating current determined from LTE emission spectroscopy.

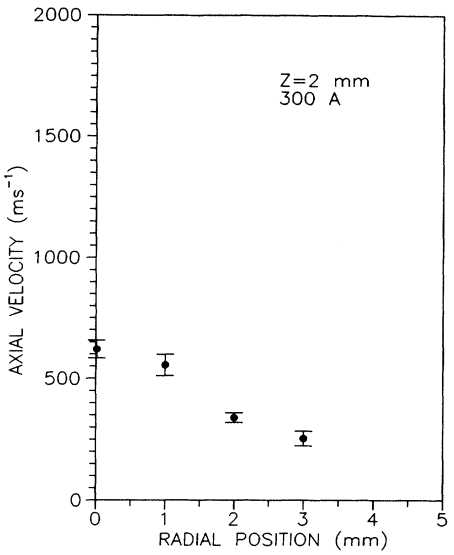

FIG. 15. Velocity distribution for 300-A operating current.

current. Radial electron density profiles calculated from the neutral Ar 714.7 and 430.0-nm emission temperature data using the excited-state Saha equation and the equation of state are plotted in Figs. 13 and 14 for the 500- and 900-A operating currents. The uncertainty in the centerline values of the electron densities is about 25%. From Figs. 10, 11, 13, and 14 it is seen that the increase in T_e and n_e with current is greater than the experimental error, while Fig. 12 shows that the gas temperature remains constant within experimental error. Apparently, the increased electrical energy goes into increasing the electron temperature and, because of the increased electron density, the total potential energy of electron-ion pairs and has little effect on raising the gas temperature or velocity. The disagreement between the centerline values of T_i and T_e at 500 A is less than the experimental error for all three spectral lines. However, at 900 A T_e and T_i agree only for the 430.0-nm emission data. While this is not conclusive, it suggests that the plasma is driven away from LTE as the current is increased. The above observations are important to understanding the kinetics of thermal plasmas and must be verified by direct measurements of the electron temperature and density from line-shape analysis of the electron feature of Thomson-scattered light.

Velocity versus radius profiles for three currents are shown in Figs. 15–17. Until now, reliable exit-plane velocity profile data have not been available. By analogy

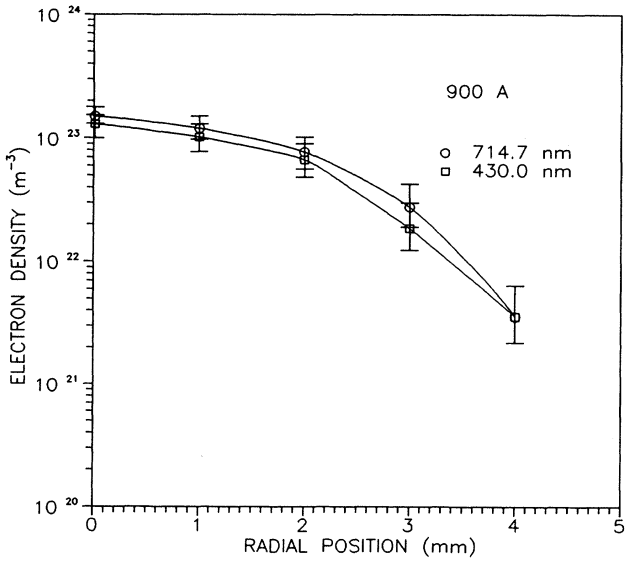

FIG. 14. Radial electron density profile for 900-A operating current determined from LTE emission spectroscopy.

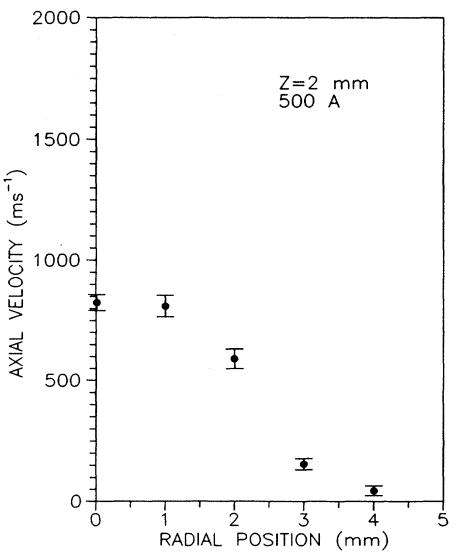

FIG. 16. Velocity distribution for 500-A operating current.

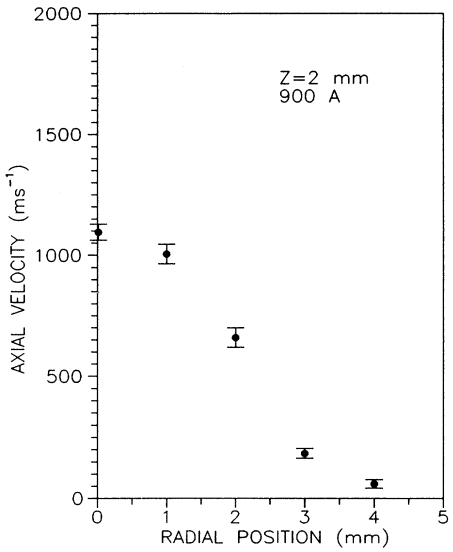

FIG. 17. Velocity distribution for 900-A operating current.

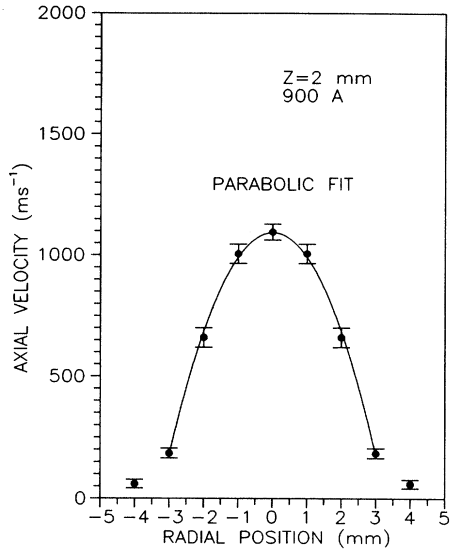

FIG. 18. Parabolic fit of 900-A velocity profile.

with incompressible laminar flow in a cylindrically symmetric channel, computational modelers postulate [11] that the velocity profiles are nearly parabolic. To examine this, the 900-A velocity data from $r=0$ to 3 mm was fit to a parabola after being reflected about the flow axis, and is plotted in Fig. 18. As can be seen, the fit is quite good and justifies the assumption of parabolic velocity profiles.

CONCLUSIONS

Using a narrow-band injection-seeded Nd:YAG laser and scanning tandem Fabry-Pérot interferometer, high-quality line-shape measurements of Thomson- and Rayleigh-scattered light were made from which gas temperature and velocity profiles of a thermal argon plasma were directly determined with uncertainties of better than 5% in many cases.

A comparison of line-shape temperature profiles with temperature profiles made using LTE emission spectroscopy shows a significant departure from LTE in the outer regions of the jet. The centerline values of gas temperature and velocity saturate as the torch operating current increases above 600 A. Emission spectroscopy shows centerline values of electron temperature and density continue to increase with current. Apparently, increasing the electrical power supplied to the torch beyond a certain point drives the plasma away from LTE. The relationship between the electron temperature and density and torch current will be studied further by analyzing the electron component of Thomson-scattered light.

To our knowledge, exit-plane temperature and velocity profiles of a thermal plasma jet have until now never been determined from line-shape analysis of scattered laser light. Temperature and velocity profiles at the torch exit are important boundary conditions for computational modeling of the plasma jet. The results of this work show that gas-velocity profiles are parabolic in the core of the jet, as sometimes postulated.

ACKNOWLEDGMENTS

This work was supported by the U.S. Department of Energy, Office of Energy Research, Office of Basic Energy Sciences, under DOE Field Office, Idaho, Contract No. DE-AC07-76ID01570.

[1] P. D. Scholz and T. P. Anderson, J. Quant. Spectrosc. Radiat. Transfer **8**, 1411 (1968).
[2] G. N. Haddad and A. J. D. Farmer, Welding J. **64**, 339s (1985).
[3] K. C. Hsu, K. Etemadi, and E. Pfender, J. Appl. Phys. **54**, 1293 (1983).
[4] H. R. Griem, *Plasma Spectroscopy* (McGraw-Hill, New York, 1964).
[5] T. Fujimoto and R. W. P. McWhirter, Phys. Rev. A **42**, 6588 (1990).
[6] M. Numano, J. Quant. Spectrosc. Radiat. Transfer **43**, 311 (1990).
[7] L. E. Cram, L. Poladian, and G. Roumeliotis, J. Phys. D **21**, 418 (1988).
[8] A. J. D. Farmer and G. N. Haddad, Appl. Phys. Lett. **45**, 24 (1984).
[9] J. Heberlein, Ph.D. dissertation, University of Minnesota, Minneapolis, 1975.
[10] C. H. Kruger, T. Owano, and M. Gordon, Pure Appl. Chem. **62**, 1833 (1990).
[11] A. N. Mostovych and A. W. DeSilva, Phys. Rev. Lett. **53**, 1563 (1984).
[12] J.-L. Lachambre, R. Decoste, A. Robert, and P. Noël, J. Appl. Phys. **57**, 1609 (1985).
[13] M. Irie and M. R. Barrault, J. Phys. D **10**, 1599 (1977).
[14] A. W. Koch, G. K. Forster, K. D. Landes, and G. Seeger in *Proceedings of the International Conference on Phenomena in Ionized Gases XX, Barga, Italy, 1991,* edited by V.

Palleschi and M. Vaseli (Institute of Atomic and Molecular Physics-CNR, Pisa, Italy, 1991), Vol. 3, p. 823.
[15] A. Goehlich, V. Schulz-von der Gathen, and H. F. Döbele, Plasma Phys. Controlled Fusion **33**, 29 (1991).
[16] A. H. Dilawari, J. Szekely, J. Batdorf, B. Detering, and C. B. Shaw, Plasma Chem. Plasma Processing **10**, 321 (1990).
[17] R. Spores and E. Pfender, in *Proceedings of the National Thermal Spray Conference, Cincinnati, OH, 1988,* edited by D. L. Houck (ASM International, Metals Park, OH, 1988), p. 85.
[18] H. J. Kunze, in *Plasma Diagnostics,* edited by W. Lochte-Holtgreven (American Elsevier, New York, 1968).
[19] T. P. Hughes, *Plasmas and Laser Light* (Wiley, New York, 1975).
[20] J. Sheffield, *Plasma Scattering of Electromagnetic Radiation* (Academic, New York, 1975).
[21] E. E. Salpeter, Phys. Rev. **120**, 1528 (1960).
[22] D. E. Evans and J. Katzenstein, Rep. Prog. Phys. **32**, 207 (1969).
[23] R. Cattolica, F. Robben, and L. Talbot, in *Proceedings of the AAIA 14th Aerospace Sciences Meeting, Washington, D.C., 1976* (American Institute of Aeronautics and Astronautics, New York, 1976), paper No. 76-31.
[24] J.-L. Lachambre, R. Decoste, and A. Robert, IEEE Trans. Plasma Sci. **PS-15**, 261 (1987).
[25] A. A. Offenberger and R. D. Kerr, Phys. Lett. **37A**, 435 (1971).
[26] M. S. Grewal, Phys. Rev. **134**, A86 (1964).
[27] S. C. Snyder and J. D. Grandy, in *Proceedings of the 28th National Heat Transfer Conference, Minneapolis, MN, 1991,* edited by K. Etemadi and J. Mostaghimi (American Society of Mechanical Engineers, New York, 1991), HTD-Vol. 161, p. 95.
[28] Z. Wang and R. J. Kearney, J. Quant. Spectrosc. Radiat. Transfer **44**, 39 (1990).
[29] S. C. Snyder, K. Etemadi, M. Roberts, and J. D. Grandy, in *Proceedings of the 10th International Symposium on Plasma Chemistry, Bochum, Germany, 1991,* edited by U. Ehlemann, H. G. Lergon, and K. Wiesemann (International Union of Pure and Applied Chemistry, Bochum, Germany, 1991), Vol. 1, p. 1.2-8.
[30] J. R. Sandercock, in *Light Scattering in Solids III, Topics in Applied Physics,* edited by M. Cardona and G. Güntherodt (Springer-Verlag, Berlin, 1982), Vol. 51.
[31] J. M. Vaughan, *The Fabry-Perot Interferometer* (Hilger, Philadelphia, 1989).
[32] S. C. Snyder, Ph.D. dissertation, University of Idaho, Moscow, 1992.
[33] J. R. Fincke (private communication).
[34] J. D. Grandy and B. A. Detering (unpublished).